Lab on a Chip

Accepted Manuscript

This article can be cited before page numbers have been issued, to do this please use: D. Spencer, F. Caselli, P. Bisegna and H. Morgan, *Lab Chip*, 2016, DOI: 10.1039/C6LC00339G.

ROYAL SOCIETY OF CHEMISTRY

www.rsc.org/loc

Journal Name

ARTICLE TYPE

Cite this: DOI: 10.1039/xxxxxxxxxx

High accuracy particle analysis using sheathless microfluidic impedance cytometry†

Daniel Spencer,‡[a] Federica Caselli,‡[b] Paolo Bisegna,*[b] and Hywel Morgan*[a]

Received Date
Accepted Date

DOI: 10.1039/xxxxxxxxxx

www.rsc.org/journalname

This paper describes a new design of microfluidic impedance cytometer enabling accurate characterization of particles without the need for focusing. The approach uses multiple pairs of electrodes to measure the transit time of particles through the device using two simultaneous differential current measurements, a transverse (top to bottom) current and an oblique current. This gives a new metric that can be used to estimate the vertical position of the particle trajectory through the microchannel. This parameter effectively compensates for the non-uniform electric field in the channel that is an unavoidable consequence of the use of planar parallel facing electrodes. The new technique is explained and validated using numerical modelling. Impedance data for 5, 6 and 7 μm particles are collected and compared with simulations. The method gives excellent Coefficient of Variation in (electrical) radius of particles of 1% for a sheath less configuration.

1 Introduction

Microfluidic Impedance Cytometry (MIC) is a widely used label-free technique for high throughput single-cell electrical analysis and discrimination[2–4]. The impedance of single particles is measured by applying an AC voltage to two pairs of electrodes and measuring the differential current as a cell transits through the system. A voltage is applied at several different frequencies and the change in current is analysed to determine the cell dielectric properties. Microfluidic impedance cytometry has been used to analyse micro-organisms[5–7], erythrocytes[8,9], leukocytes[10,11], platelets[12,13], and animal and human cell lines[14–16]. Low frequency (e.g. 500 kHz) impedance is used to size particles because at these frequencies (and in high conductivity buffer) the particle volume is related to the real part of the complex impedance signal, in a similar manner to a Coulter volume measurement. At higher frequencies, the electrical impedance is influenced by the cell membrane and the cytoplasmic properties. For the widely used parallel electrode geometry (Figure 1(a)), the measured impedance signal also depends on the position of the particle between the electrodes, i.e. the trajectory of the particle as it flows through the channel. This is because the electric field in the channel is not uniform and the particle can influence the current in the reference arm of the sensor[1]. This manifests itself as an error in the measured "volume" of the particle for off-centre particles (i.e. close to the top or bottom electrodes).

To obtain high quality (low CV) data, nearly all cytometers use some form of particle focusing. Typically, particles are focused using sheath flow[17], first introduced in 1968 for the Coulter counter[18]. However, sheath flow focusing increases the complexity of the system (in particular for 2-D focusing in planar geometries)[17] and consumes significant additional fluid. Microfluidic particle focusing has also been demonstrated using Dean flows[19] and inertial focusing[20–22]. Inertial focusing requires high flow rates and is highly dependent on particle size, so that measurement of heterogeneous populations becomes difficult. Externally applied forces can also be used to focus particles within the fluid. For example dielectrophoresis[6,23] (DEP) and acoustophoresis[24] have been used to focus particles without the use of a secondary flow. Other novel approaches include combining DEP and inertial microfluidics[25]. In sheath-less focusing systems, the magnitude of the force on a particle (hence the focused position) depends on the physical properties of the particle including volume and intrinsic physical/electrical properties. This means that it can be difficult to optimise any given system for a heterogeneous sample.

Particle focusing is not generally used in MIC; particles move through the analysis region between the electrodes in a random manner that reflects the parabolic nature of pressure driven flow. However, this causes errors in the measurement signals when particles flow near the electrodes[1]. Using multiple pairs of electrodes, the SNR can be increased[26,27], and the interaction with immobilised surface antigens can be studied[28], however the vari-

[a] School of Electronics and Computing Science, University of Southampton, Highfield, Southampton, SO17 1BJ, UK. E-mail: hm@ecs.soton.ac.uk
[b] Department of Civil Engineering and Computer Science, University of Rome Tor Vergata, 00133 Rome, Italy. E-mail: bisegna@uniroma2.it

† Electronic Supplementary Information (ESI) available. See DOI: 10.1039/b000000x/

‡ These authors contributed equally to this work.

View Article Online
DOI: 10.1039/C6LC00339G

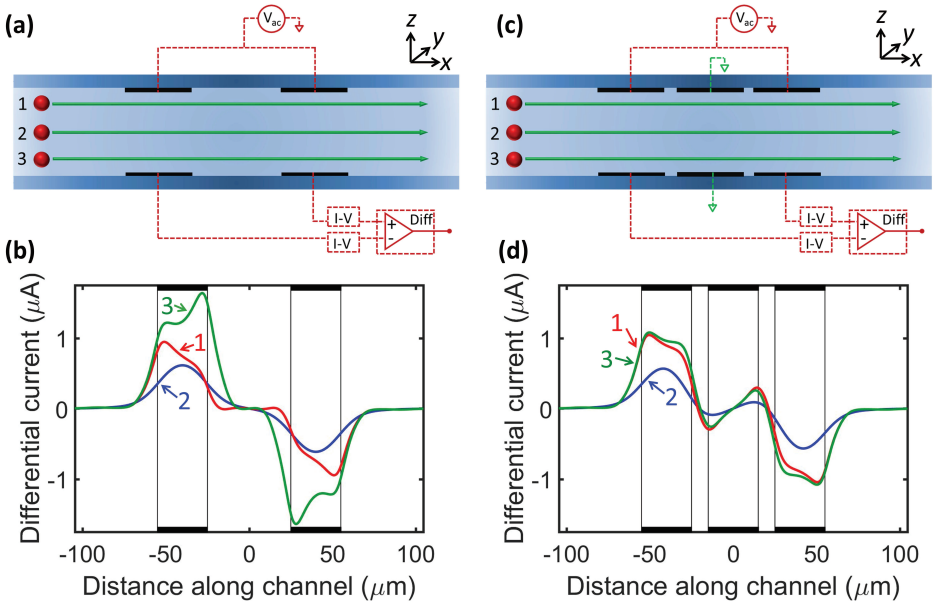

Fig. 1 (a) Diagram showing the structure of a parallel facing electrode microfluidic impedance cytometer. (b) Simulated differential currents for an insulating 7 μm diameter particle passing through the measurement region (36 μm wide and 45 μm high, 30 μm wide electrodes separated by 50 μm) with three different trajectories: close to the top electrodes (3 μm gap, curve 1), through the middle of the channel (curve 2) and close to the bottom electrodes (3 μm gap, curve 3). Curves 1 and 3 are different due to an asymmetry in the current flow between the electrode pairs[1]. (c) shows a new electrode design where a pair of grounded electrodes are positioned between the measurement pairs to prevent current flow between the measurement electrode pairs (30 μm wide separated by 10 μm). The simulated differential signal is shown in (d). Parameter values used for the simulations are reported in the ESI†.

ation in signal with particle position still remains an issue that limits the accuracy of impedance cytometry. In this work, we describe a simple approach to compensate for the variation in signal caused by the random position of a particle. A new chip design coupled with a signal-processing compensation strategy is demonstrated. The technique is based on a new metric that enables an estimate of the vertical position of the particle from a simultaneous oblique current measurement.

2 Operating principle

Figure 1(a) shows the widely used parallel facing 4-electrode design. Particles are suspended in an electrolyte (e.g. PBS) and are pumped through the channel at a typical flow rate of 40 μl/min in a 40 μm $\times$ 40 μm channel giving a maximum particle velocity of the order of 1 m/sec. The impedance signal exhibits an antisymmetric shape[1,29], as shown in the figure. The peak voltage signal is recorded and is used to determine the dielectric properties of the particle at that frequency[2]. As discussed in the introduction, the electric field within the channel is non-uniform and therefore the magnitude of the measured electrical current depends on particle position. Figure 1(b) shows that not only is the signal magnitude different, but also the shape of the signal in the top or bottom half of the channel is different. This asymmetry is caused by a cross current that flows between diagonally opposite electrodes that is modulated when the particle passes[1].

The velocity of a particle flowing through the channel can be determined from the transit time, defined as the time between the positive and negative impedance peaks. The transit time reflects the position of a particle in the channel, i.e. those near the walls move more slowly than particles travelling in the centre (Figure S1(a)†). However, it is not possible to determine the *y*-*z* spatial position of a particle from the transit time; only its radial position. As shown in Figure 1(b) (see also Figure S1(b)†), the impedance signal for an identical particle varies with the vertical position in the channel (*z*-axis), and consequently the impedance "error" cannot be corrected using transit time information alone.

To reduce the magnitude of the cross current and reduce the error in impedance signal, ground electrodes can be introduced into the system as shown in Figure 1(c). These grounded electrodes remove the cross currents from diagonally opposite electrodes, reducing the positional dependence of the impedance signal. However, this method does not completely eliminate the error, as shown by the simulated signal of Figure 1(d) (see also Figure S2(a)†). Signals from the off-centre particles are still higher than those flowing in the centre of the chip (the lower the electrode-width to channel-height ratio, the higher this effect, Figure S3†). Knowledge of the particle *z*-position in the channel is therefore required to uniquely correct for the height-dependent impedance variation. This can be achieved by including two pairs of additional measurement electrodes at each end of the system as shown in Figure 2. These electrodes provide a second and independent transit time measurement at an oblique angle (Δt_{OBQ}) compared with the transverse (top to bottom) transit time, Δt_{TSV}. Both the transverse and oblique transit times depend on flow rate and cell position in the channel but the ratio of Δt_{OBQ} to Δt_{TSV} only depends on the particle height. This ratio can be used to provide an independent measurement of particle height which can be used to correct for the impedance signal.

View Article Online
DOI: 10.1039/C6LC00339G

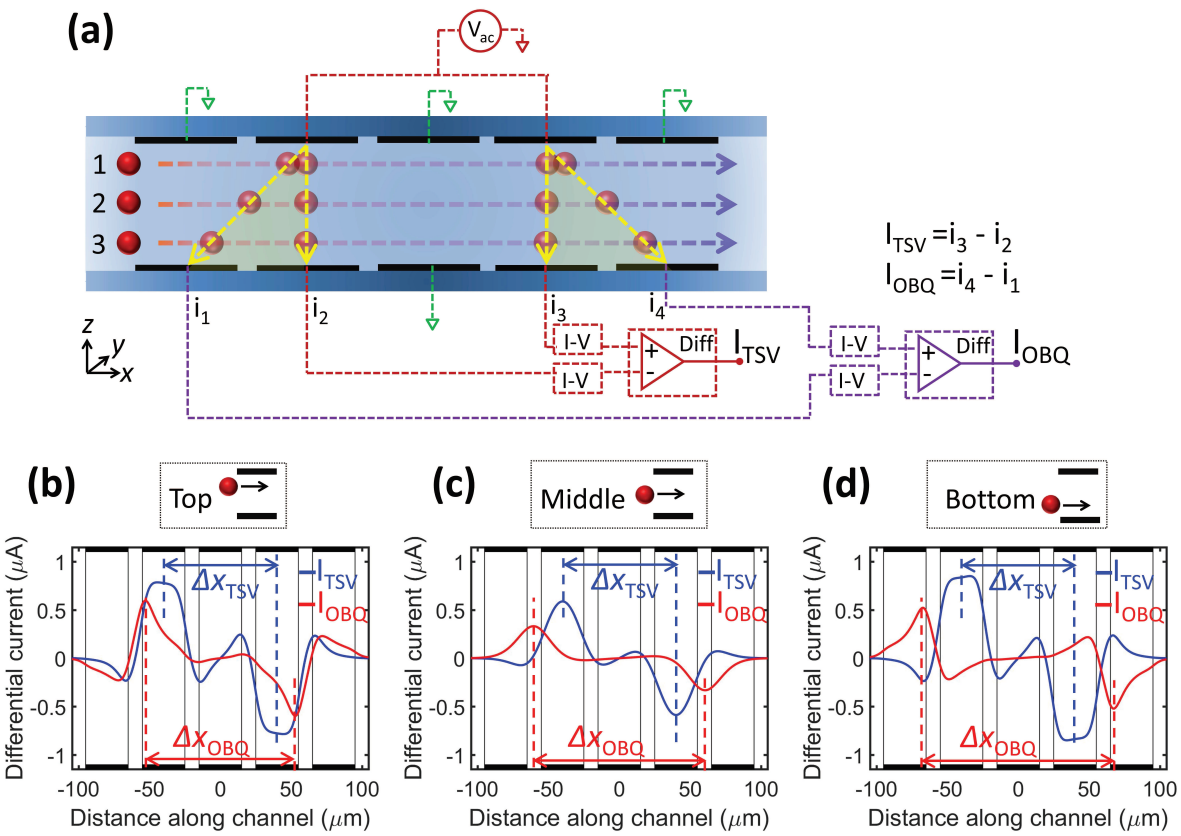

Fig. 2 (a) Diagram of the improved electrode design which has an additional measurement electrode pair either side of the 6 electrodes of Figure 1(c). Two differential current measurements are made: a transverse measurement (I_{TSV}) and an oblique measurement (I_{OBQ}). (b)-(d) show simulated transverse (blue line) and oblique (red line) signals for 7 μm diameter beads passing close to the top electrodes (3 μm gap), through the centre, and close to the bottom of the channel (3 μm gap). Parameter values used for the simulations are reported in ESI†.

View Article Online
DOI: 10.1039/C6LC00339G

The system was characterised using finite element simulations to determine the field and current – details of the computational model of a typical impedance cytometer can be found elsewhere [1,30–32] (also see ESI†). The simulations were performed using the dimensions of the actual experimental microfluidic chip, which had a channel with approximate dimensions of 36 μm (wide) × 45 μm (high), with 30 μm wide electrodes and 10 μm spacing, and using the electrical parameters shown in Table S1†. Figure 2(b)–(d) shows the real part of the simulated transverse impedance (blue) and oblique impedance (red) for a 7 μm diameter insulating spherical particle. The three figures show the impedance for particles close to the top (3 μm gap), (b) in the centre, and (c) close to the bottom (3 μm gap). Both the transverse I_{TSV}, and oblique differential current I_{OBQ}, is plotted in the figure for identical particles. For all three particle heights, the peak position for the transverse current corresponds to approximately* the mid-points of the measurement electrodes (2nd and 4th pairs). The distance between peaks (Δx_{TSV}) is the same in all three cases (80 μm). The oblique current peaks occur at different positions as shown in the figure (red), where Δx_{OBQ}=105 μm, 120 μm and 135 μm for Figure 2(b)–(d) respectively. The particle transit time Δt depends on particle velocity, but the ratios ($\Delta x_{OBQ}/\Delta x_{TSV}$) and consequently ($\Delta t_{OBQ}/\Delta t_{TSV}$) are dimensionless numbers that relate to particle height in the channel, independent of velocity (Figure S2(b)†). This metric can therefore be used to correct the signal impedance for off-centre particles.

3 Experimental

Microfluidic chips were fabricated as described elsewhere [12]. Metal electrodes were lithographically patterned onto glass substrates and channels were made from SU8 using full wafer bonding in bonder. Individual chips were diced from bonded wafers. The channels had cross sectional dimensions of 36 μm (wide) × 45 μm (high). Fluidic and electrical connections were made to the chips using a custom 3-D printed acrylic block. Polystyrene beads with diameters of 5, 6 and 7 μm (Sigma-Aldrich and Polysciences) were re-suspended to a concentration of approximately 500 beads per μl in PBS containing 0.1% Tween 20 and sufficient sucrose to match the density of the suspending medium to the density of the particles (1050 kg/m^3). Particles were pumped through the device with a syringe pump at a flow rate of 40 μl/min. Impedance was measured using a Zurich Instruments transimpedance amplifier (HF2TA, 10kΩ gain) and impedance scope (HF2IS, 50 kHz filter bandwidth). A signal of 4 V at 1 MHz was applied to two top electrodes and the transverse and oblique differential currents were sampled at 230k samples per second. Data was processed using custom software written in Matlab.

4 Results

Figure 3 shows a scatter plot for 7 μm diameter beads, with the dimensionless ratio $\Delta t_{OBQ}/\Delta t_{TSV}$ plotted against the cube root of the impedance magnitude at 1 MHz (proportional to particle diameter). The impedance is multiplied by a gain factor to account for the electronic circuitry. Particles with the smallest impedance have a value of $\Delta t_{OBQ}/\Delta t_{TSV}$ of approximately 1.5. This value closely matches the simulations of Figure 2(b) where the ratio ($\Delta x_{OBQ}/\Delta x_{TSV}$) is 120 μm/80 μm = 1.5. These particles are located in the mid-point of the channel. Particles passing close to the top or bottom of the channel have a different values of $\Delta t_{OBQ}/\Delta t_{TSV}$, with higher impedance signals (see simulations in Figure 2). Examples of experimental single particle impedance signals are shown in Figure 3, along with arrows indicating the position of the particle on the scatter plot. Also shown in the figure (yellow stars) are the values obtained from numerical simulations for the same channel geometry demonstrating excellent correlation.

Table 1 Fitting parameters of model equation $X = a[1+b(Y-c)^2]$.

	a	b	c
5 μm	4.92	1.60	1.50
6 μm	5.96	1.54	1.50
7 μm	6.96	1.54	1.50
Mean	-	**1.56**	**1.50**

Figure 4(a) to (c) shows a density plot of $\Delta t_{OBQ}/\Delta t_{TSV}$ vs particle diameter (cube root of impedance) for three different bead sizes (measured separately), along with data for a mixed population, in Figure 4(d). In each case the same parabolic trend is observed. This data can be fitted to a scaled $X = Y^2$ function:

$$X = a[1+b(Y-c)^2], \quad (1)$$

where a is particle diameter, and the constants b and c account for the variation in signal with particle height as determined from the ratio $\Delta t_{OBQ}/\Delta t_{TSV}$. Parameters b and c are determined from the electrode geometry, with c the ratio of $\Delta t_{OBQ}/\Delta t_{TSV}$ at the mid-point (i.e. 1.5) and b accounts for the change in impedance peak height as particles move off centre, and reflects the electrode-width to channel-height ratio. These fitting parameters are listed in Table 1, and the corresponding parabolas are shown in red in Figure 4. The constants, b and c should be independent of particle sizes, which is clear from Table 1 where the difference are minor. The mean value for constants b and c was then used to calculate the parabolas shown in Figure 4(d) for the three different particle sizes, showing an excellent fit with the data. The consistency in the constants along with the fit in Figure 4(d) demonstrates that this method can be used to correct any experimental data for variations in particle height for a given channel size and electrode geometry.

Figure 5(a) and (b) shows histograms for the data sets shown in Figure 4, for both individual particle populations and the mixed sample. As expected the distribution has a significant spread and skew, as reported previously [1]. Equation (1) was used to correct the raw data as follows:

$$|Z_{corrected}|^{1/3} = \frac{|Z_{measured}|^{1/3}}{1+b(Y-c)^2}, \quad (2)$$

* Note that the absolute maximum of the peak shifts slightly due to the slight asymmetry in the shape of the peak. However, the peak of a Gaussian template is measured, not the absolute maximum.

View Article Online
DOI: 10.1039/C6LC00339G

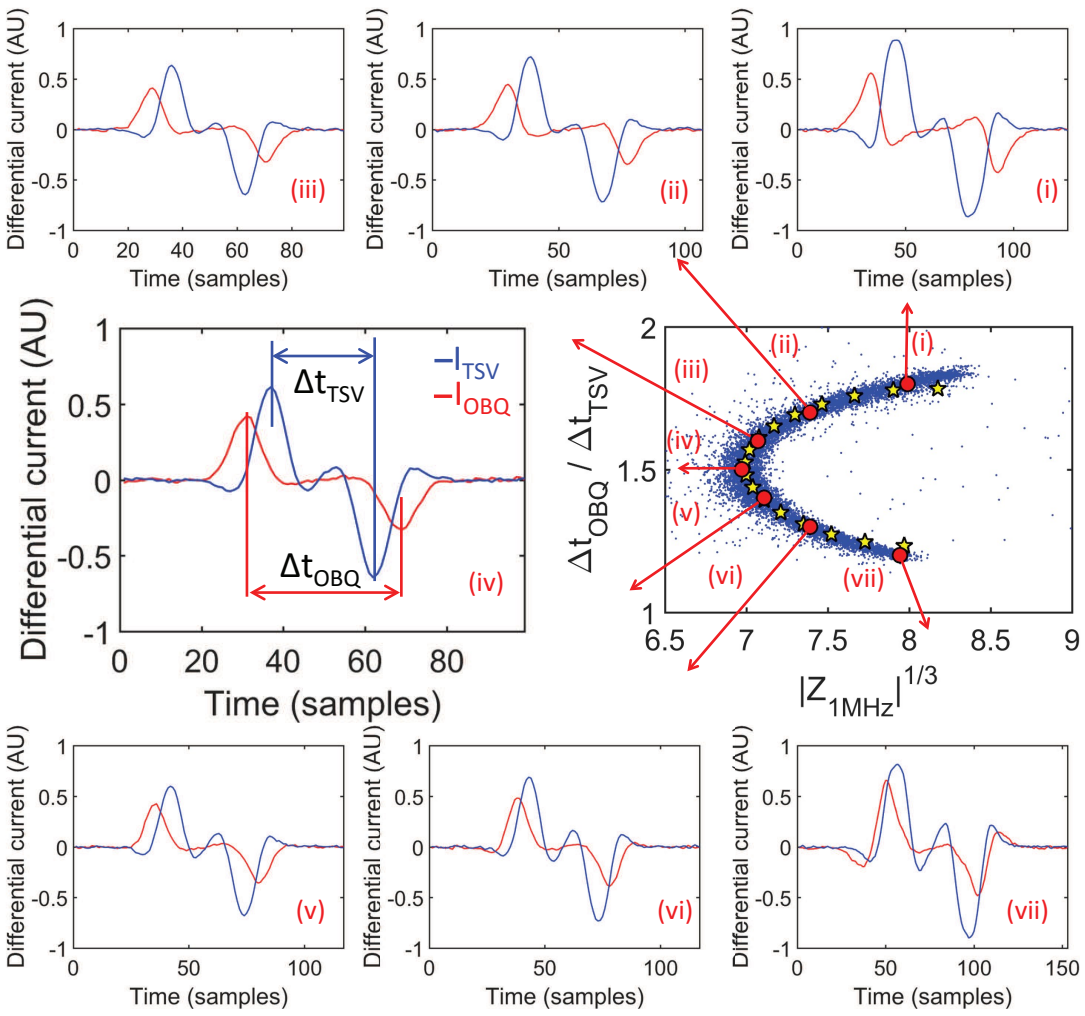

Fig. 3 Middle-right: scatter plot for 7 μm diameter beads, with the dimensionless ratio $\Delta t_{OBQ}/\Delta t_{TSV}$ plotted against the cube root of the impedance magnitude at 1 MHz (proportional to particle diameter). Impedance is multiplied by a single gain factor to account for the electronic circuitry. The yellow stars are the values obtained from numerically simulated differential current for the actual dimensions of the chip used in the experiment (36 μm wide and 45 μm high). (i)-(vii) are experimental single particle impedance signals for the red data points in the scatter plot.

View Article Online
DOI: 10.1039/C6LC00339G

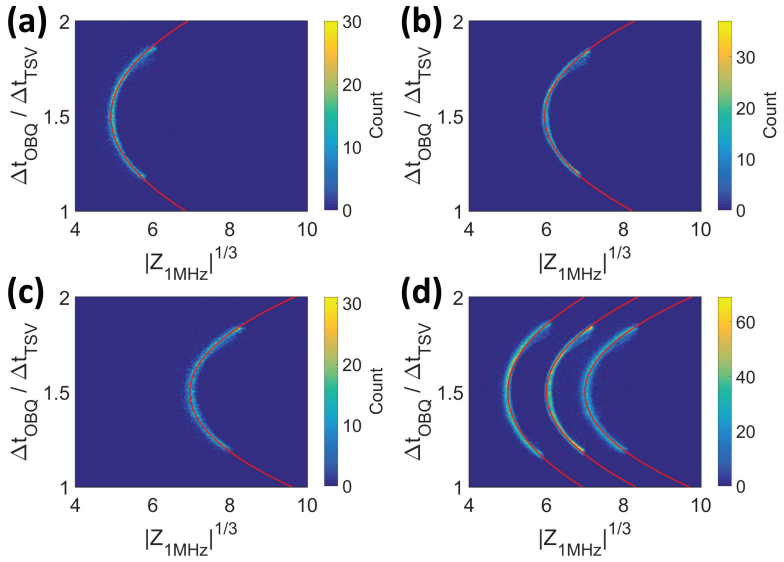

Fig. 4 Density plot for populations of beads of different sizes, with the dimensionless ratio $\Delta t_{OBQ}/\Delta t_{TSV}$ plotted against the cube root of the impedance magnitude at 1 MHz (proportional to particle diameter). (a) 5 μm diameter beads, (b) 6 μm diameter beads, (c) 7 μm diameter beads and (d) a mixture of 5, 6 and 7 μm diameter beads measured together. The fitted parabolas $X = a[1 + b(Y - c)^2]$ are shown as red lines. For each population, parameter values a, b, and c are reported in Table 1. In (d), the three parabolas are defined with $a = 5.0$, 6.0, 7.0 and the same parameters b and c (average values, Table 1).

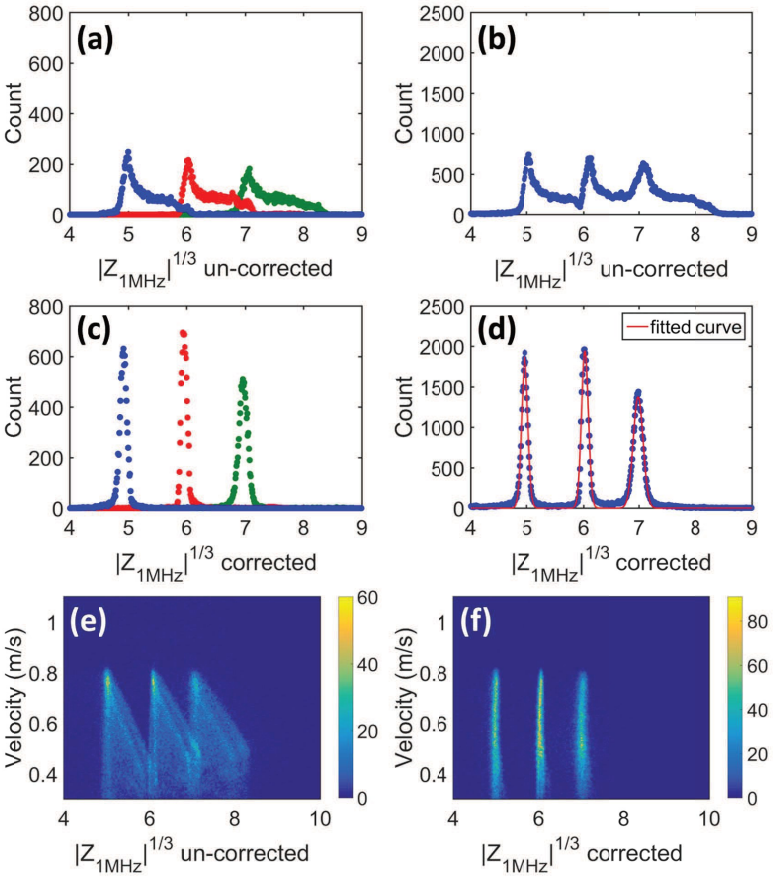

Fig. 5 Histogram of the impedance of 5, 6 and 7 μm diameter beads measured (a) separately and (b) together. (c)-(d) show the corrected data has an almost perfect Gaussian distribution. (e) and (f) show density plots of particle velocity vs impedance for the mixture of beads before and after correction. In (f) each population of beads has the same impedance regardless of velocity and therefore position in the channel.

View Article Online
DOI: 10.1039/C6LC00339G

where $Y = \Delta t_{OBQ}/\Delta t_{TSV}$ and b and c are the mean values of the constants in Table 1. The corrected data is plotted in Figure 5(c) and (d) showing an almost perfect Gaussian distribution (as expected). Fitting a Gaussian allows the CVs to be calculated as follows: 1.27%, 0.99%, and 1.24%, for the 5, 6, and 7 μm diameter beads respectively. This can be compared with the manufacturers' quoted values of 1.8%, 7.5%† and 1.7%. Figure 5(e) and (f) show density plots of particle velocity vs impedance for the mixture of beads (raw data in (e) and corrected data in (f)), demonstrating that this simple algorithm completely eliminates the height dependent variation in impedance, i.e. all particles of a given size range have the same impedance irrespective of trajectory through the channel. For these corrections, the mean value of the parameter b was used. The CVs were also calculated for the range of b shown in Table 1 (1.5 to 1.6) and found to change marginally, to a maximum of 1.29% for the 5 μm diameter beads (b = 1.6).

Although the absolute magnitude of b and c solely depends on channel geometry, an optimal design of microfluidic chip and electrode configuration is governed by a number of conflicting constraints. These includes: (i) maximising the absolute signal – this requires a shallow channel but places an upper limit on particle size and can lead to clogging; (ii) minimising coincidence[33] whilst maximising throughput, but this requires a small interrogation volume (small electrodes close together). This reduces the signal magnitude, especially at low frequencies where the response is limited by the electrical double layer capacitance.

5 Conclusions

This paper describes a new design of microfluidic impedance cytometer chip together with a signal processing algorithm that gives high quality impedance signals without the need for any particle focusing. The design minimises the variation in the measured magnitude of the impedance signal for off-centre particles. Further signal processing using simple techniques completely eliminates this error. Post-processing the data is quick, and can be done in close to real time. The design therefore solves one of the fundamental limiting issues in the application of parallel facing electrode arrangement for high accuracy and quality data collection. It will enable new applications of microfluidic impedance cytometry technology; for example an impedance-based diagnostic system would not require storage and control of additional fluids for flow focusing. Although a number of microfluidic flow-focusing technique have been used for cytometry, the forces typically scale with particle volume or even size to forth-power, meaning that these techniques are challenging for small particle or heterogeneous mixtures. Our approach requires trivial calibration of a given chip geometry, together with a simple algorithm to correct the impedance signals that is independent of particle size and flow rate.

† The 6 μm diameter beads from PolySciences have a much higher reported CV than the 5 μm and 7 μm obtained from Sigma Aldrich. The value is clearly incorrect.

6 Acknowledgements

This work was supported by the Scientific Independence of Young Researchers Programme (SIR 2014) under Grant RBSI14TX20-MUSIC "Multidimensional Single-Cell Microfluidic Impedance Cytometry". HM wishes to acknowledge the award of a Royal Society Industry Fellowship. The data from this paper can be obtained from the University of Southampton repository at `http://dx.doi.org/10.5258/SOTON/TBC`.

References

1 D. Spencer and H. Morgan, *Lab Chip*, 2011, **11**, 1234–39.
2 T. Sun and H. Morgan, *Microfluid. Nanofluid.*, 2010, **8**, 423–43.
3 K. C. Cheung, M. Di Berardino, G. Schade-Kampmann, M. Hebeisen, A. Pierzchalski, J. Bocsi, A. Mittag and A. Tárnok, *Cytometry Part A*, 2010, **77**, 648–66.
4 J. Chen, C. Xue, Y. Zhao, D. Chen, M. Wu and J. Wang, *Int. J. Mol. Sci.*, 2015, **16**, 9804–9830.
5 C. Bernabini, D. Holmes and H. Morgan, *Lab Chip*, 2011, **11**, 407–412.
6 N. Haandbaek, O. With, S. C. Burgel, F. Heer and A. Hierlemann, *Lab Chip*, 2014, **14**, 3313–3324.
7 M. Shaker, L. Colella, F. Caselli, P. Bisegna and P. Renaud, *Lab Chip*, 2014, **14**, 2548–55.
8 K. Cheung, S. Gawad and P. Renaud, *Cytometry Part A*, 2005, **65A**, 124–32.
9 C. Küttel, E. Nascimento, N. Demierre, T. Silva, T. Braschler, P. Renaud and A. G. Oliva, *Acta. Trop.*, 2007, **102**, 63–8.
10 D. Holmes, D. Pettigrew, C. H. Reccius, J. D. Gwyer, C. van Berkel, J. Holloway, D. E. Davies and H. Morgan, *Lab Chip*, 2009, **9**, 2881–2889.
11 D. Spencer, G. Elliott and H. Morgan, *Lab Chip*, 2014, **14**, 3064–3073.
12 C. van Berkel, J. D. Gwyer, S. Deane, N. Green, J. Holloway, V. Hollis and H. Morgan, *Lab Chip*, 2011, **11**, 1249–1255.
13 M. Evander, A. J. Ricco, J. Morser, G. T. A. Kovacs, L. L. K. Leung and L. Giovangrandi, *Lab Chip*, 2013, **13**, 722–9.
14 H. L. Gou, X. B. Zhang, N. Bao, J. J. Xu, X. H. Xia and H. Y. Chen, *J. Chromatogr. A*, 2011, **1218**, 5725–9.
15 J. L. Hong, K. C. Lan and L. S. Jang, *Sens. Act. B Chem.*, 2012, **173**, 927–34.
16 H. Song, Y. Wang, J. M. Rosano, B. Prabhakarpandian, C. Garson, K. Pant and E. Lai, *Lab Chip*, 2013, **13**, 2300–10.
17 X. Xuan, J. Zhu and C. Church, *Microfluid. Nanofluid.*, 2010, **9**, 1–16.
18 L. Spielman and S. Goren, *J. Colloid Interface Sci.*, 1968, **26**, 175–182.
19 X. Mao, A. Nawaz, S. Lin, M. Lapsley, Y. Zhao, J. McCoy, W. El-Deiry and T. Huang, *Biomicrofluidics*, 2012, **6**, 024113.
20 D. Di Carlo, *Lab Chip*, 2009, **9**, 3038–3046.
21 S. Hur, H. Tse and D. Di Carlo, *Lab Chip*, 2010, **10**, 274–280.
22 J. Kim, J. Lee, C. Wu, S. Nam, D. Di Carlo and W. Lee, *Lab Chip*, 2016, **16**, 992–1001.

View Article Online
DOI: 10.1039/C6LC00339G

23 D. Holmes, H. Morgan and N. Green, *Biosens. Bioelectron*, 2006, **21**, 1621–1630.

24 C. Grenvall, C. Antfolk, C. Bisgaard and T. Laurell, *Lab Chip*, 2014, **14**, 4629–4637.

25 J. Zhang, S. Yan, G. Alici, N. Nguyen, D. Di Carlo and W. Li, *RSC Adv.*, 2014, **4**, 62076–62085.

26 S. Emaminejad, S. Talebi, R. W. Davis and M. Javanmard, *IEEE Sens. J.*, 2015, **15**, 2715–2716.

27 D. Polling, S. C. Deane, M. R. Burcher, C. Glasse and C. H. Reccius, 14th International Conference on Miniaturized Systems for Chemistry and Life Sciences, MicroTAS, 2010.

28 K. R. Balakrishnan, J. C. Whang, R. Hwang, J. H. Hack, L. A. Godley and L. L. Sohn, *Anal. Chem.*, 2015, **87**, 2988–2995.

29 F. Caselli and P. Bisegna, *IEEE Trans Biomed Eng*, 2016, **63**, 415–422.

30 T. Sun, N. G. Green, S. Gawad and H. Morgan, *IET Nanobiotechnol.*, 2007, **1**, 69–79.

31 F. Caselli, P. Bisegna and F. Maceri, *J. Microelectromech. Syst.*, 2010, **19**, 1029–40.

32 F. Caselli, M. Shaker, L. Colella, P. Renaud and P. Bisegna, *J. Microelectromech. Syst.*, 2014, **23**, 785–794.

33 U. Hassan and R. Bashir, *Lab Chip*, 2014, **14**, 4370–81.